Analysis of the Expansion-Fan Flowfield for Holes in a Hypersonic Configuration

John J. Bertin*
University of Texas at Austin, Austin, Texas
and
William J. Tedeschi,† Daniel P. Kelly,† Albino C. Bustamante,‡ and Eric W. Reece‡
Sandia National Laboratories, Albuquerque, New Mexico

An investigation has been conducted to define the viscous/inviscid flowfield that results when an external, supersonic flow encounters an opening in the surface of a hypersonic vehicle. Pitot probes and Mach-flow-angularity probes provided data for the external boundary-layer and free-shear-layer/expansion-fan flow that occurs when a wedge containing a cavity is exposed to the Mach 8 stream of Tunnel B of the Arnold Engineering Development Center. A numerical code has been developed using the rotational method-of-characteristics for a nonadiabatic flow in order to generate flowfield solutions for comparison with these data. Using the ratio of the internal cavity pressure to the external surface presssure (p_c/p_e) as an input boundary condition, there is good agreement between the computations and the data for the pitot-pressure profiles and the flow directions in the free-shear-layer/expansion-fan flow.

Nomenclature

L = length (in the plane-of-symmetry) of the ESP
M_∞ = the freestream Mach number (8 for AEDC Tunnel B)
p_{t1} = stagnation pressure in the wind-tunnel reservoir
p_{t2} = stagnation pressure downstream of a normal shock wave
$\dot{q}$ = heat-transfer rate
R = gas constant
s = entropy
T_t = total temperature (not necessarily equal to the total temperature of the freestream flow)
T_{t1} = total temperature in the wind-tunnel reservoir
U_∞ = freestream velocity
$(du_e/ds)_t$ = stagnation-point velocity gradient for the recompression face
x = distance from the leading edge of the model
$\tilde{x}$ = distance from the departure lip of the ESP
z = vertical distance from the surface of the wedge
$z_{rcf,i}$ = z-coordinate of the inner surface of the recompression face
$z_{rcf,o}$ = z-coordinate of the outer surface of the recompression face
$z_{t,le}$ = thickness of the leading edge of the ESP (i.e., the departure lip)
γ = ratio of specific heats
δ_w = wedge deflection angle
θ = flow direction
μ = Mach wave angle
$\tilde{\rho}$ = dimensionless density (ρ/ρ_e)

Subscripts

c = value in the cavity
e = value of the inviscid flow at the edge of the (departure) boundary layer
rec = value at the recompression face
w = value at the wall

Presented as Paper 88-0373 at the AIAA 26th Aerospace Sciences Meeting, Reno, NV, Jan. 11-14, 1988; received Jan. 28, 1988; revision received Sept. 12, 1988.

*Bettie Margaret Smith Professor of Engineerings; currently with Sandia National Laboratories. Fellow AIAA.
†Member of the Technical Staff. Member AIAA.
‡Division Supervisor.

Introduction

VEHICLES entering the Earth's atmosphere are subjected to a severe aerothermodynamic environment. If there is an opening in the surface that allows flow into the interior cavities of the reentry vehicle (RV), the complex viscous interactions that are produced can cause increases in the aerodynamic loads and locally severe increases in heating. If a tile or a portion of the Space Shuttle Orbiter were to be inadvertantly lost, the increased severity of the aerothermodynamic environment could jeopardize the mission of the Orbiter. In other instances, a foreign object could impact the surface of the reentry vehicle with such force as to damage the surface of the RV. Other surface openings (or surface ports) may be designed into reentry vehicles, and proper account must be taken of the internal heating within these cavities. The effect of surface openings on the aerothermodynamic environment has been the subject of numerous investigations, e.g., Ref. 1.

A multiphase test program has been conducted in Tunnel B of the Arnold Engineering Development Center (AEDC) in which a wedge model was exposed to the Mach 8 stream. The model design was such that a circular external surface port (ESP) could be located in the wedge surface, exposing an internal cavity to the external flow. In addition, two vents located in the back plate of the model could be opened, exposing the air in the internal cavity to the low pressure base region. Thus, with the external surface port and the two base vents open, the air adjacent to the wedge surface, i.e., the external flow, could pass through the ESP into the cavity and out the base vents. Data were obtained to define the aerothermodynamic environment in and around the ESP.

A numerical code has been developed to calculate the flowfield in the expansion fan using the rotational method-of-characteristics (RMOC) for a nonadiabatic flow. The integral momentum equation was used to calculate the pressure acting on the downstream, or recompression, face of the ESP. A modified stagnation-point heating analysis was used to calculate the "average" heat-transfer rate for the recompression face.

The computed aerothermodynamic environments for the recompression face of the ESP were compared in detail with experimental data in Ref. 2. Similar comparisons were made

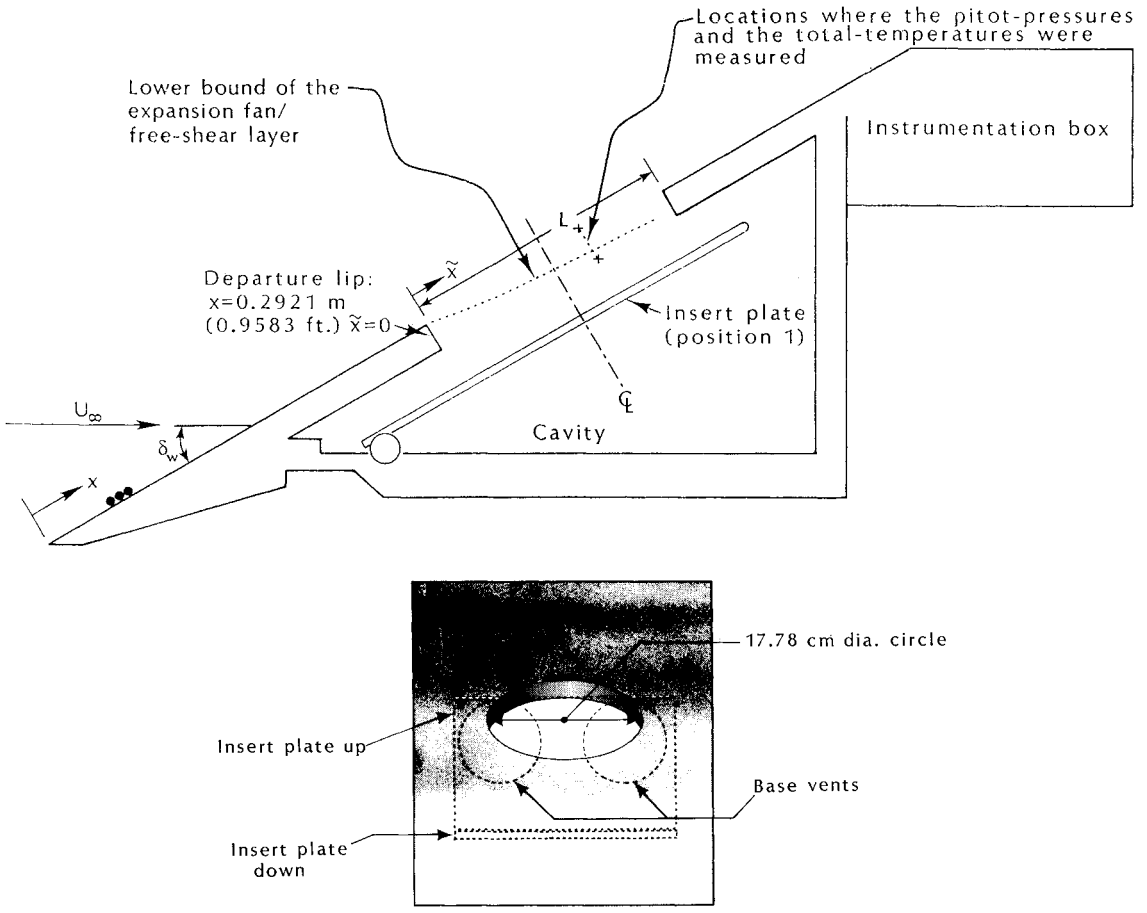

Fig. 1 Sketch of the wedge configuration with 0.1778-m-long ESP with insert plate up (position 1).

for the external boundary layer and for the expanded flow.[3] The correlations for the entire flowfield are summarized in the present paper.

Experimental Program

The experimental data discussed in the present paper were obtained in a multiphase program conducted in Tunnel B at AEDC. A semiwedge model was exposed to the Mach 8 stream. By changing the inclination of the model support sting, data were obtained with nominal wedge angles (δ_w) of 17 and 24 deg. This allowed variation of the shock-layer flow properties without changing the freestream flow. The nominal Reynolds number of the freestream flow was 1.07×10^6/m with corresponding stagnation reservoir conditions of

$$p_{t1} = 5.85 \times 10^6 \text{ N/m}^2, \qquad T_{t1} = 750 \text{ K}$$

A sketch of the semiwedge model is presented in Fig. 1. The wedge (or external) surface was 0.6096 m long and 0.4318 m across. The cavity extended the width of the model. The model design was such that the plate forming the external surface could be changed. The data presented herein were obtained for a wedge surface in which there was a single, circular opening whose diameter was 17.78 cm and whose center was 0.3810 m from the leading edge of the external surface.

Three rows of steel balls were used to "trip" the external boundary layer to ensure that it was turbulent at the departure lip of the ESP. The middle row of the trips was located 5.08 cm from the leading edge. The balls were either 0.0635 or 0.0991 cm in diameter. The spacing between rows was approximately 3.5 sphere diameters, as was the lateral spacing between the balls of a row. The balls in each successive row were offset 1.17 diameters from the balls in the row immediately in front of them. The size of the trips was calculated based on the correlations presented in Ref. 4. Heat-transfer data obtained during preliminary tests conducted at the outset of the test program verified that the tripped boundary layer was turbulent.

The mass flow rate through the cavity could be increased by opening two vent ports located in the base of the model (see Fig. 1). Opening the base vents allows the cavity to vent to the low-pressure base region. Data were obtained both with the vents completely sealed (i.e., no base venting) and with them open. The open vent ports were either 5.08 or 10.16 cm (4.00 in.) in diameter. A moveable insert plate was located in the cavity in order to change the internal geometry and, therefore, alter the flow through the cavity. For the present tests, the insert plate was either parallel to the external surface (position 1), which is shown in Fig. 1, or down—parallel to the bottom of the cavity (position 3).

The principal objective of the present investigation was the development of a computer code that could be used to generate solutions of the free-shear-layer/expansion-fan flowfield and the recompression region. Wind-tunnel tests were conducted to obtain data for comparison with the computed flowfield parameters. In one phase of the test program, a Mach-flow-angularity (MFA) probe[5] was used to measure pitot pressures and the flow directions within the expanding flow. These measurements were obtained in the plane-of-symmetry of the ESP, 11.71 cm downstream of the departure lip (which is approximately two-thirds of the ESP diameter). In the second phase of the test program, pitot-pressure probes and total temperature probes were located at the same station in the range of coordinates shown in Fig. 1. For reference, the lower bound of the expansion fan, as computed using the RMOC code, is also presented in Fig. 1.

Theoretical Analysis

For a vehicle flying through the atmosphere at hypersonic speeds, the shock-layer flow is locally supersonic over exten-

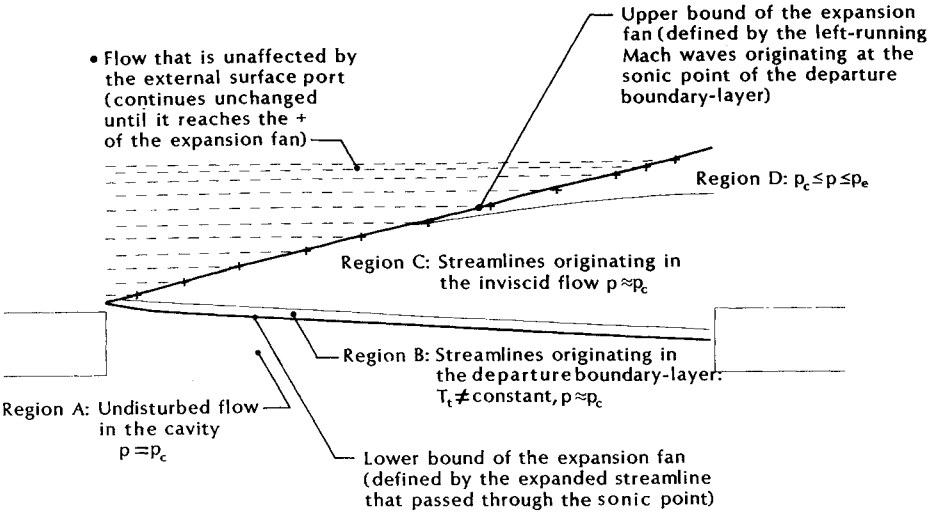

Fig. 2 Sketch of the expansion flowfield for supersonic flow past an external surface port with $p_c = 0.722p_e$, $\delta_w = 17$ deg, $L = 0.1778$ m.

sive regions of the vehicle. If this locally supersonic flow encounters an opening in the surface of the vehicle so that the cavity is contained in a "notch," both the separation and recompression points are fixed. When the cavity is relatively deep, the external flow spans the notch entirely and is designated an "open cavity flow." If the internal flow were truly "dead" and the dividing streamline isobaric, the pressure in the cavity would be constant. Charwat notes: "Experiment shows that, indeed, this is grossly true when the cavity length to depth ratio is small (less than 4)."[6] This is essentially true even for the more complicated cavity configurations of interest to the present study, where the cavity pressure is essentially constant except in regions where the ingested flow impinges on internal surfaces.

In the present study, for the base-vented configurations, the flow through the base vents was choked. As a result, the mass efflux through the base vents was proportional to the cavity pressure (p_c). This mass efflux must be equal to the mass entering the cavity through the external surface port. Thus, the external flow is turned as it encounters the ESP. Inward rotation of the external flow is accompanied by a reduction in the static pressure of the fluid entering the cavity. Furthermore, the pressure level in the "open" cavity and the deflection imposed on the external flow by the geometry of the cavity boundaries are interrelated in order that the mass balance is satisfied.

Because the cavity pressure (p_c) is less than the external pressure at the departure lip of the ESP (p_e), i.e., the cavity-pressure-ratio (p_c/p_e) is less than one, an "expansion fan" results as the flow encounters the cavity. As shown in Fig. 2 (which represents a computed flowfield), the lower bound of the expansion fan is the streamline passing through the sonic point of the departure boundary layer, while the upper bound of the expansion fan is the trace of the left-running characteristics from the nodal points at the upper end of the expansion fan (starting at the sonic point). The present flow model neglects the diffusion of shear forces in the free shear layer. As a result, there is a discontinuity in the computed velocity field at the interface between the quiescent cavity flow (region A of Fig. 2) and the expanded flow originating in the departure boundary layer (region B). In reality, viscous forces would cause the supersonic flow in the expanding external stream to entrain air from the cavity. However, several researchers[7] have found that the spreading rate, i.e., the growth rate of the mixing region, is much smaller for compressible, supersonic flows than for incompressible flows. Furthermore, as will be noted when discussing the present data, neglecting the entrainment of the quiescent fluid within the cavity resulted in relatively small differences between the pitot-probe measurements from the shear layer and the computed values of p_{t2}. Hence,

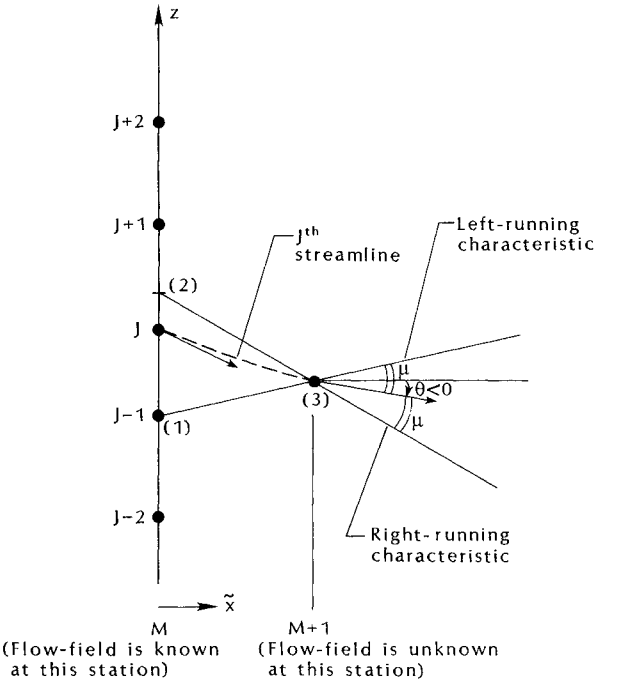

Fig. 3 Sketch of the characteristics (and nomenclature) used in computed flow along the Jth streamline.

neglecting the diffusion of shear forces in the free shear layer is a reasonable approximation for the present flows.

Thus, the flow model for the expansion fan assumes that the diffusion of viscous forces in the expanding flow is negligible, that the entropy remains constant along a streamline, and that the flow is steady and two-dimensional. The agreement between the computed flow parameters and the corresponding measured values that are presented in this paper support the validity of these assumptions. The differential equation of the hodograph characteristics is

$$\pm d\theta = \sin\mu \cos\mu \frac{dp}{\rho} + \frac{\sin\mu \cos\mu(\gamma - 1)}{\gamma} \frac{ds}{R} \tag{1}$$

The physical characteristics make a Mach angle with respect to the velocity vector:

$$\left(\frac{dz}{d\tilde{x}}\right) = \tan(\theta \pm \mu) \tag{2}$$

In these two equations, the upper sign corresponds to the right-running characteristics and the lower sign corresponds to the left-running characteristics.

A flowfield solution is generated in planes of constant $\tilde{x}$, starting from the plane of the departure lip ($\tilde{x} = 0$), which serves as the upstream boundary. The flow properties at $\tilde{x} = 0$ are input, having been computed using another computer code. With the flowfield known in the (M) plane, i.e., $\tilde{x} = \text{const}$, a solution is computed for the ($M + 1$) plane, i.e., $\tilde{x} + \Delta\tilde{x}$ (see Fig. 3). The solution algorithm follows the streamlines, starting with the streamline that originated at the sonic point. Since the cavity-pressure-ratio (p_c/p_e) serves as a boundary condition and since the entropy is assumed constant along a streamline, these two properties uniquely define the flow along the lower boundary. Thus, the flow direction can be computed using only the right-running characteristic of Eq. (1).

The geometry of the solution algorithm for a typical internal flowfield point is illustrated in the sketch of Fig. 3. By moving along a streamline, e.g., the Jth streamline, the entropy at point 3, i.e., point ($M + 1, J$), is equal to that at point (M, J). Characteristics are projected from point 3 back to the M plane, where the intersection of the right-running characteristic is point 2 and that of the left-running characteristic is point 1. Manipulating linearized forms of Eq. (1), expressions for $\tilde{\rho}_3$ and θ_3 can be obtained:

$$\tilde{\rho}_3 = \exp\left\{\left[(\theta_1 - \theta_2) + \ell n\tilde{\rho}_2\left(\sin\mu\cos\mu\Big|_2^3\right) + \ell n\tilde{\rho}_1\left(\sin\mu\cos\mu\Big|_1^3\right) - \frac{(\gamma-1)}{\gamma}\left(\sin\mu\cos\mu\Big|_2^3\right)\left(\frac{s_3}{R} - \frac{s_2}{R}\right) - \frac{(\gamma-1)}{\gamma}\left(\sin\mu\cos\mu\Big|_1^3\right)\left(\frac{s_3}{R} - \frac{s_1}{R}\right)\right] \Bigg/ \left[\left(\sin\mu\cos\mu\Big|_2^3\right) + \left(\sin\mu\cos\mu\Big|_1^3\right)\right]\right\} \tag{3}$$

$$\theta_3 = \left[(\theta_1 + \theta_2) + \left(\sin\mu\cos\mu\Big|_2^3\right)\ell n\frac{\tilde{\rho}_3}{\tilde{\rho}_2} - \left(\sin\mu\cos\mu\Big|_1^3\right)\ell n\frac{\tilde{\rho}_3}{\tilde{\rho}_1} + \frac{(\gamma-1)}{\gamma}\left(\sin\mu\cos\mu\Big|_2^3\right)\left(\frac{s_3}{R} - \frac{s_2}{R}\right) - \frac{(\gamma-1)}{\gamma}\left(\sin\mu\cos\mu\Big|_1^3\right)\left(\frac{s_3}{R} - \frac{s_1}{R}\right)\right] \Big/ 2 \tag{4}$$

The flowfield in the expansion fan is computed by marching in the streamwise direction using this computational procedure for the nonadiabatic RMOC. The sketch (to scale) of a computed expansion-fan flowfield for an external surface port (Fig. 2) illustrates the essential features of the computed flow: region A, the quiescent, undisturbed flow in the cavity; region B, containing those streamlines originating in the departure boundary layer; region C, containing streamlines that originated in the inviscid flow and where $p \approx p_c$; and region D, containing streamlines that originated in the inviscid flow but where the local pressure varies between p_c and p_e. An additional point is incorporated at the upper bound of the new ($M + 1$) plane, where the flow properties are assumed to be equal to the values at the departure lip (i.e., station 1) and therefore are (as yet) unchanged by the expansion.

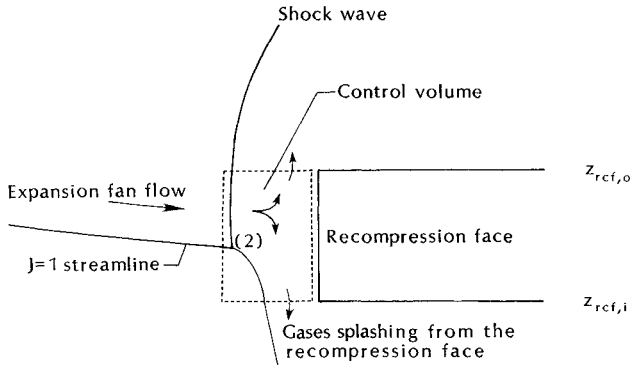

Fig. 4 Sketch of the impinging flow in the vicinity of the recompression face.

When the supersonic flow of the expansion fan encounters the recompression face of the external surface port, a shock wave is generated, decelerating the flow and producing significant increases in the temperature and in the pressure of the flow impinging on the recompression face. For the current solution algorithm, the integral momentum equation was applied to the control volume of Fig. 4 in order to compute the pressure acting on the recompression face. To compute the heat-transfer rate to the recompression face, the approach of Fay and Riddell[8] was modified for use in the present application. The flow in the shock layer adjacent to the recompression surface is assumed to be similar to a "stagnation region" flow. Treating the flow in this region as a two-dimensional stagnation-region flow past a blunt body, the correlations of Boisson and Curtiss[9] were used to compute the equivalent nose radius for the recompression face. Nestler notes that "ample evidence exists that the impingement heat flux from turbulent shear layers exceeds the theoretical laminar stagnation point heat flux because of local freestream turbulence effects."[10] Citing data from the literature, Nestler presented a correlation of experimental to theoretical heat flux to be applied to two-dimensional turbulent shear layers. A linearized fit of the correlation presented in Fig. 2 of Ref. 10 was used in computing F_{turb}, the factor to compensate for the assumed turbulence in the approach flow. Combining these concepts, the "stagnation-point" heat-transfer rate ($\dot{q}_{\text{rec}}$) was computed as:

$$\dot{q}_{\text{rec}} = 0.6767[(\rho_{\text{rec}}\mu_{\text{rec}})^{0.4}(\rho_w\mu_w)^{0.1}] \times [c_p(T_{\text{rec}} - T_w)]\sqrt{\left(\frac{du_e}{ds}\right)_t}\,F_{\text{turb}} \tag{5}$$

Comparisons Between Computation and Experiment

External Flow

Measurements of the local static pressures and of the local heat-transfer rates and shadowgraphs were used to define experimentally the external flowfield. Data were obtained for smooth-plate configurations and with transition-fixing boundary-layer trips located 5.08 cm from the leading edge. A collage of 1) a schematic diagram of the basic flowfield, 2) a shadowgraph, and 3) a typical pitot pressure profile across the shock layer is presented in Fig. 5. Insights into the external flow can be gained by examining the information presented in this figure. Since the trips were sized to ensure that they would be effective in promoting boundary-layer transition, they are roughly the same size as the local boundary-layer thickness. Thus, when the external flow encountered the trips, a strong viscous/inviscid interaction including shock waves was generated. When this trip-induced shock wave intersects the bow shock wave, a strong slip line (or shear layer) is produced that can be seen parallel to the top plate in the shadowgraph. The trips produce a pitot pressure "defect" in the boundary layer (region 1 of Fig. 5), i.e., the measured total pressures are less than the computed values over a considerable fraction of the boundary layer. Furthermore, a vortical (mixing) flow was created by the expansions and vortices associated with the flow over the spherical trips (region 2). The pitot pressures measured in this region exhibited an S-shaped defect (see Fig. 5c), even though the flowfield computations and the total-temperature measurements indicated that this region is outside of the boundary layer.

Rather than generate a boundary-layer solution for each run using the specific test conditions for that run when analyzing

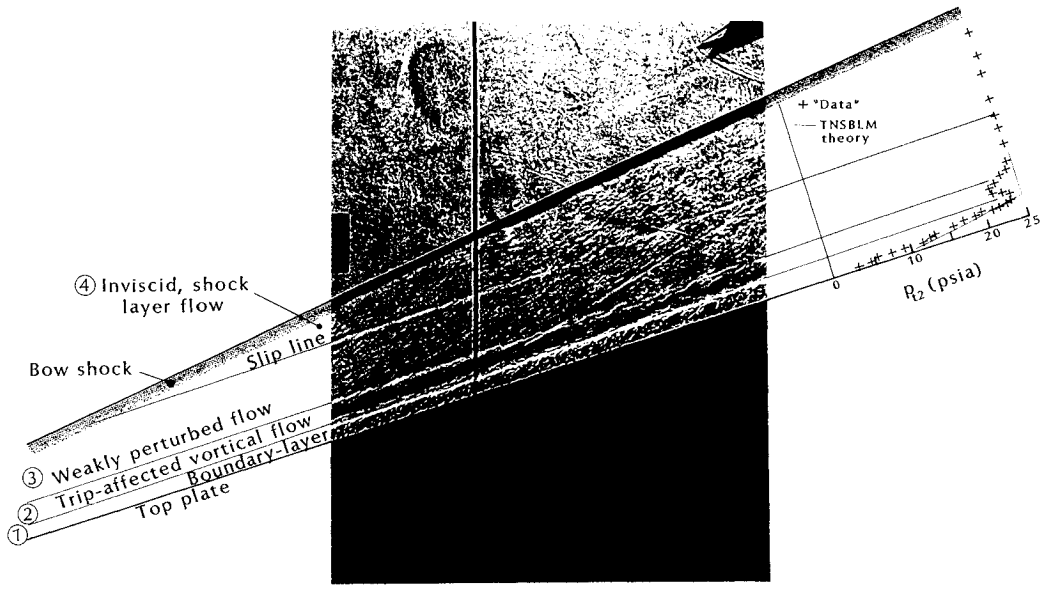

(a) Schematic diagram of the basic flow field (b) Shadowgraph (c) Typical pitot-pressure profile

Fig. 5 Collage depicting the characteristics of the external shock-layer flowfield.

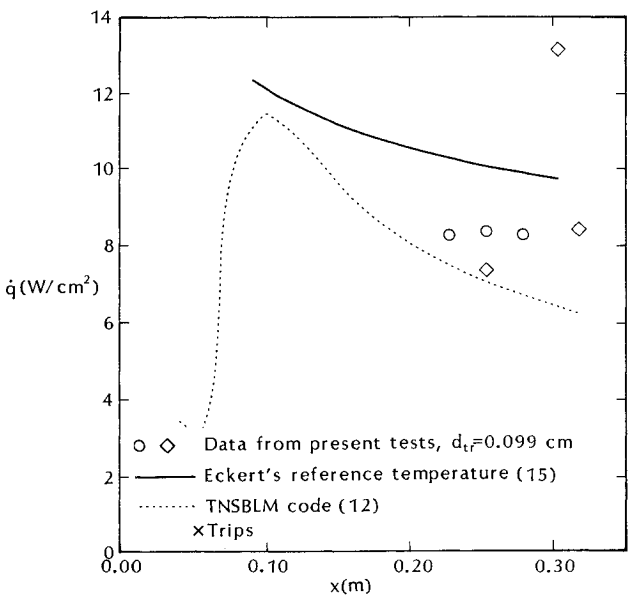

Fig. 6 Heating rate distribution on the wedge surface, δ_w = 24 deg.

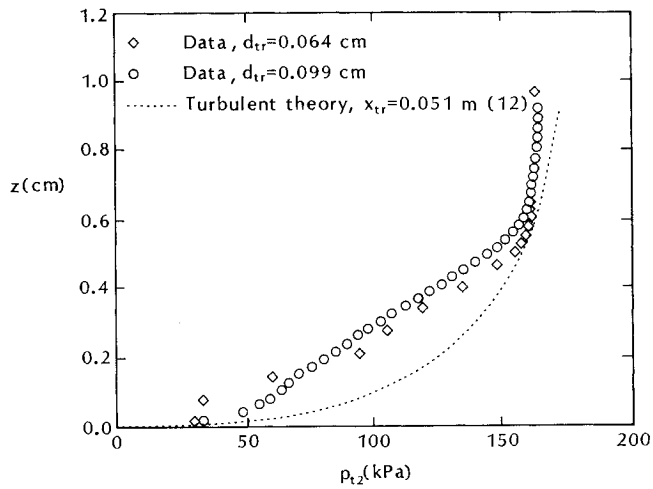

Fig. 7 Comparison of experimental and computed pitot-pressure profiles for the external boundary layer at x = 0.292 m, δ_w = 24 deg.

the data, it was decided to choose one flow condition as representative of the test conditions. The parameters for the reference flow condition were:

$$M_\infty = 8, \qquad p_{t1} = 5.732 \times 10^6 \text{ N/m}^2$$

$$T_{t1} = 749.8 \text{ K}, \qquad T_w = 350 \text{ K}$$

Once p_{t1}, T_{t1}, M_∞, and δ_w had been specified, all other parameters defining the inviscid flowfield were calculated using the charts and tables of Ref. 11. For δ_w = 17 deg, $p_e = 7.16 \times 10^3$ N/m^2 and $M_e = 4.272$. For $\delta_w = 24$ deg, $p_e = 1.23 \times 10^4$ N/m^2 and $M_e = 3.163$. The pressures measured at an orifice 0.279 m from the leading edge ranged from 1.038 to 1.046 times the theoretical value for δ_w = 17 deg and from 1.100 to 1.107 times the theoretical value for δ_w = 24 deg.

Theoretical solutions for the boundary layer along the wedge surface were obtained using the TNSBLM (Turbulent Non-Similar Boundary Layer, Modified) code.[12] The turbulence model in the TNSBLM code is the mixing-length/eddy-viscosity model of Cebeci and Smith.[13] Except for the solutions for which the boundary layer was constrained to be entirely laminar, the onset of transition was assumed to be at x = 5.08 cm, i.e., at the location of the boundary-layer trips. Thus, the trips were assumed to be "effective" in promoting transition. The boundary layer in the transitional region was modeled using the intermittency factor of Cebeci and Smith. For the present conditions, the x coordinate at the end of transition was somewhat greater than twice that of the onset of transition. The computed heat-transfer distributions are compared with data for δ_w = 24 deg in Fig. 6. The heat-transfer rates were measured using a Schmidt-Boelter gage, which is described in Ref. 14. The computed heat-transfer rates are at the lower bound of the data scatter. Since $y^+ = 11$ for the first node of the computed boundary layer at x = 0.305 m, the agreement between the data and the TNSBLM computations is considered very good. With the exception of the measurement at x = 0.305 m, the heating rates calculated using the Eckert reference temperature formulation[15] are significantly greater than the measured values. The heating sensed by the gage at x = 0.305 m was relatively high for all eight runs made with this ESP configuration (i.e., all three venting levels, both angles of attack, and both repeat runs).

The pitot-pressure profiles measured for δ_w = 24 deg are compared in Fig. 7 with the p_{t2} distributions derived from the

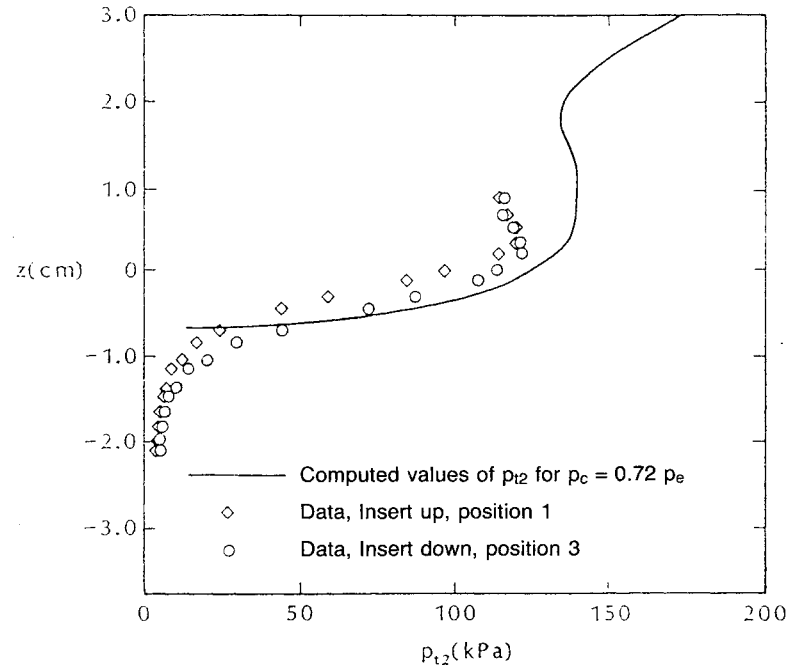

a) Pitot-pressure profiles

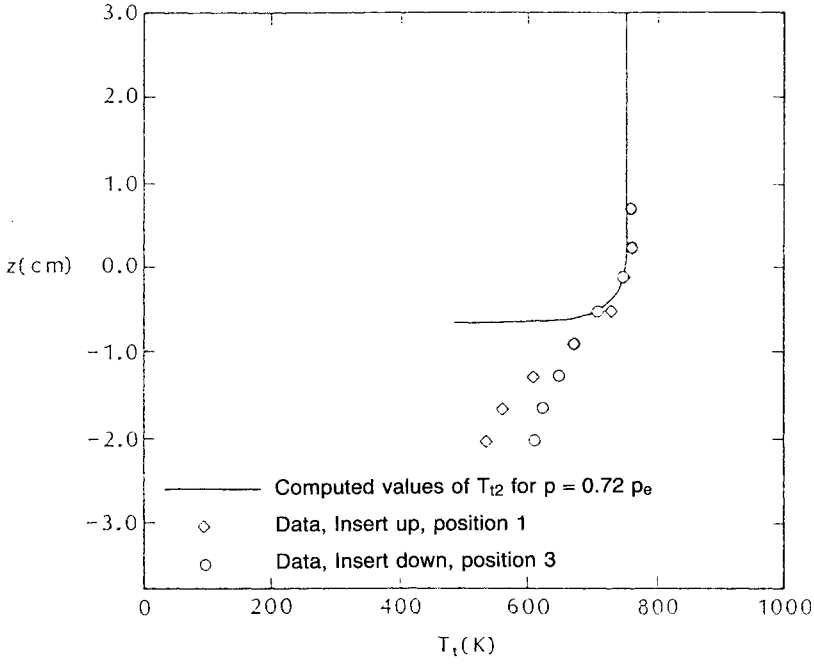

b) Total temperatures

Fig. 8. Comparison of expansion-fan data illustrating the effect of insert plate position, δ_w = 17 deg, both 10.16 cm diam base vents open, d_{tr} = 0.099 cm.

computed boundary layer. The relatively low pitot pressure measured for $z \leq 0.6$ cm are attributed to the shock-wave system and highly vortical flow caused by the presence of the boundary-layer trips. For 0.6 cm $< z \leq \delta$, there is satisfactory agreement between the pitot-probe measurements and the computed values of p_{t2}.

Despite the trip-induced pitot-pressure "defects" both within and external to the boundary layer, the agreement between the computed external flow parameters and the measured values (including the surface heat-transfer rates) was considered reasonable. Thus, the boundary layer at the departure lip (just upstream of the surface port), which serves as the upstream boundary condition for the expansion flow in the surface opening, was taken from the computations (generated using the TNSBLM code) and not from the data or from any empirically adjusted theory.

Expansion-Fan/Free-Shear-Layer Flow Measurements

Pitot-pressure profiles and total-temperature profiles for the expansion-fan/free-shear-layer flow are compared with the corresponding computed values in Fig. 8. The computed flowfield assumed the cavity-pressure-ratio to be 0.72, which was based on the measured values of p_c and p_e. These comparisons are for the δ_w = 17 deg wedge with the insert plate up (position 1) and with the insert plate down (position 3).

The upper bound for the expanded boundary-layer flow (region B of Fig. 2) is approximately $z = 0$. The computed p_{t2} variation for $z > 2.29$ cm (0.9 in.) is that for region D of Fig. 2. Comparing the pitot-pressure profiles, we see that for this configuration (with the insert in the lower position) 1) the entrainment of fluid from the cavity produces only slight increases in the pitot presssures measured for $z \leq -0.838$ cm; 2) there is excellent agreement between data and the computations near the bottom of the computed free shear layer (which neglects the entrainment of cavity flow) both in location and in magnitude; and 3) despite the trip-induced flowfield perturbations, the agreement between the data and the computations is reasonable for the expanded flow that originally was outside the boundary layer, i.e., $z > 0$.

The two sets of pitot-pressure data and the computations are in satisfactory agreement. The most significant difference between the two sets of data is the (slight) upward displace-

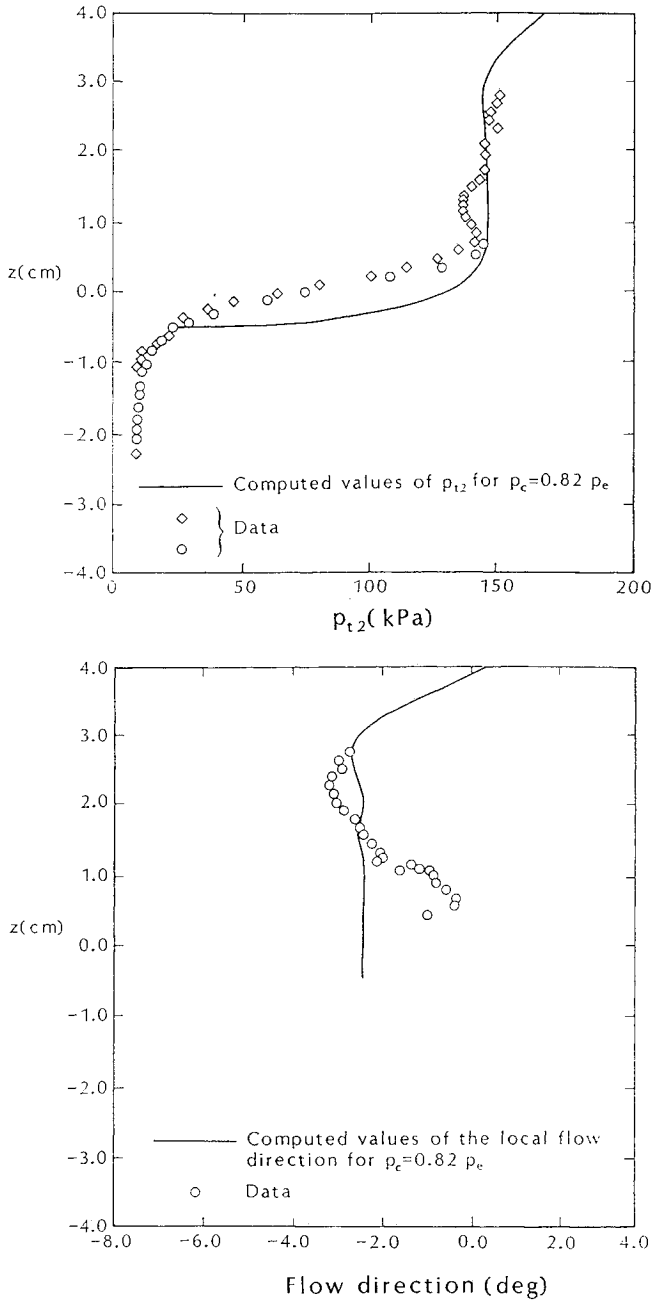

Fig. 9 Comparison of expansion-fan data with theory for δ_w = 24 deg, both 10.16 cm diam vents open, insert position 1, d_{tr} = 0.099 cm.

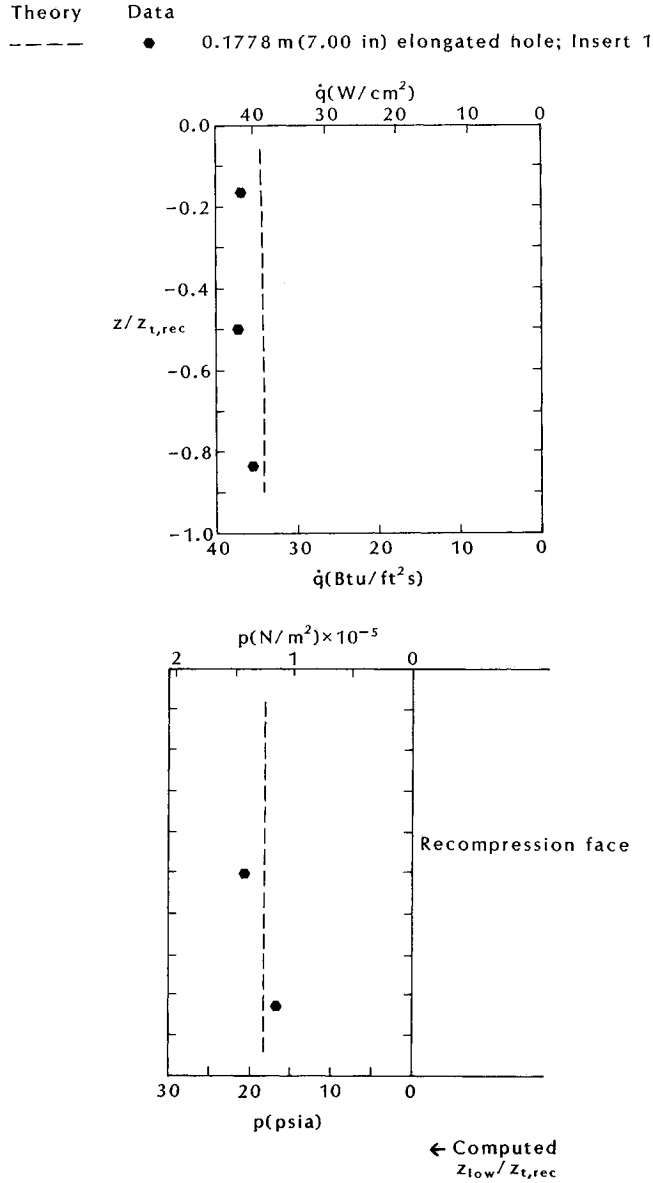

Fig. 10 Comparison of experimental and computed flow parameters on the recompression face of the 0.1778 m long ESP, δ_w = 24 deg, with both 10.16 cm diam base vents open, d_{tr} = 0.099 cm.

ment of the shear layer with the insert plate up. These data support the intuitive assumption that if the insert plate in the upper position has any affect on the cavity flow, it would be to restrict the flow causing the cavity pressure to be slightly higher.

One disturbing variance evident in these (and, in fact, in all of the current) total-temperature data is the high stagnation temperatures for $z \leq -0.914$ cm. Since pitot-probe measurements indicate that the entrainment of cavity flow is "second-order," these values of T_t appear to be unreasonably high. The authors question the validity of these four measurements. Another reason to suspect the total-temperature measurements is that, when probing the external boundary layer, the total temperature was never less than 583 K, even when the probe was within 0.018 cm of the surface (whereas the surface temperature was approximately 350 K). Furthermore, Hahn[16] presented measured local stagnation temperature in the shear layer for flow past a cavity in a hypersonic stream. The greatest decrease in local stagnation temperature occurred in the shear layer. The stagnation temperature of the reverse flow was relatively constant (since the Mach number of the reverse flow was always less than 0.2) and was only slightly higher than the cavity-wall temperature. Hahn's data are consistent with the authors' belief that the total temperature of the air in the cavity below the free shear layer should be relatively low.

Pitot-pressure profiles and flow-direction data (as determined with the MFA probe) are compared in Fig. 9 with the computed values of the parameters for the δ_w = 24 deg wedge with the insert plate up. The computed flowfield assumed the cavity-pressure-ratio to be 0.82. Since these pitot-probe data extend higher, the following additional observations are made.

1) The trip-induced "defect" observed in the external pitot-profiles from region 2 of Fig. 5 persists in the expansion fan's pitot pressures in the vicinity of z = 1.00 cm. Again, this supports the assumption that the total pressure is constant along a streamline, i.e., that viscous diffusion/dissipation is second order for the relatively short streamwise dimensions of these expanding flows.

2) The measured and computed total pressures increase in the upper region of the expansion fan (region D of Fig. 2) for $z > 2.5$ cm, since the computations indicate that the static

pressures increase in the region where the adjustment from p_c to p_e takes place.

The correlation between the experimentally determined and the computed flow directions is considered very good.

Recompression Face Parameters

The computed values of the surface pressure and the heat transfer for the recompression lip of the ESP for the $\delta_w = 24$ deg wedge with both 10.16 cm diam base vents open are compared with data in Fig. 10. As indicated by the arrow at the right of Fig. 10, the lower bound of the computed expansion fan was below the inner surface of the recompression face. Thus, the entire surface of the recompression face is immersed in the impinging flow of the expansion fan. Therefore, the data presented in Fig. 10 represent a flowfield that is most like that of the flow model used in computing the stagnation-region parameters for the recompression face. As a result of the general compatability between the computational flow model and the actual flowfield, there is very good agreement between the experimental values and the computed values both for the surface pressure and for the heat-transfer rates.

Concluding Remarks

The viscous/inviscid flowfield that results when an external, supersonic flow encounters an opening in the surface of a hypersonic vehicle has been computed using the rotational method of characteristics for a nonadiabatic flow. The flow model for the expansion fan assumes that the diffusion of viscous forces in the expanding flow is negligible, that the entropy remains constant along a streamline, and that the flow is steady and two-dimensional.

Although the relatively large trips used to ensure that the hypersonic boundary layer was turbulent produced significant flowfield disturbances, correlations between data and theory were believed to be satisfactory. Satisfactory correlations were obtained for the following parameters: 1) the static pressure and the heat-transfer-rate distributions on the external surface, 2) the pitot-pressure and the local-flow-direction profiles across the expansion fan/free-shear layer, and 3) the static pressures and the heat-transfer rates on the recompression face of the ESP. The exceptions to the satisfactory correlations between data and theory were the total temperature measurements from below the shear layer.

Acknowledgments

The authors would like to thank Robert Buffington, Robert Sheldahl, and Jose Suazo (of the Sandia National Laboratories) for providing their time and talents, which were critical to the success of the wind tunnel tests. The authors would also like to thank the Center of Excellence for Hypersonic Training and Research and Tim Valdez for administrative support.

References

[1]Hunt, L. R., "Aerodynamic Heating and Loading Within Large Open Cavities in Cone and Cone-Cylinder Flare Models at Mach 6.7," NASA TN D-7403, March 1974.

[2]Bertin, J. J., Tedeschi, W. J., Bustamante, A. C., and Reece, E. W., "The Aerothermodynamic Environment for Holes in Hypersonic Configurations," AIAA Paper 87-2631 CP, Aug. 1987.

[3]Bertin, J. J., Tedeschi, W. J., Kelly, D. P., Bustamante, A. C., and Reece, E. W., "Analysis of Shear-Layer Probe Data for Holes in Hypersonic Configurations," AIAA Paper 88-0373, Jan. 1988.

[4]Sterrett, J. R., Morrisette, E. L., Whitehead, A. H., Jr., and Hicks, R. M., "Transition Fixing for Hypersonic Flow," NASA TN D-4129, Oct. 1967.

[5]Marquardt, E. J., Stepanek, S. A., Byers, M. T., and Donaldson, J. C., "Development and Calibration of Miniature Mach/Flow-Angularity Probes," AIAA Paper 84-0630, Jan. 1984.

[6]Charwat, A. F., "Supersonic Flows with Imbedded Separated Regions," *Advances in Heat Transfer,* Academic, New York, 1970, pp. 1–131.

[7]Ikawa, H. and Kubota, T., "Investigation of Supersonic Turbulent Mixing Layer with Zero Pressure Gradient," *AIAA Journal,* Vol. 13, May 1975, pp. 566–572.

[8]Fay, J. A. and Riddell, F. R., "Theory of Stagnation Point Heat-Transfer in Dissociated Air," *Journal of the Aeronautical Sciences,* Vol. 25, Feb. 1958, pp. 73–85, 121.

[9]Boisson, J. C. and Curtiss, H. A., "An Experimental Investigation of Blunt Body Stagnation Point Velocity Gradient," *ARS Journal,* Vol. 29, Feb. 1959, pp. 130–135.

[10]Nestler, D. E., "An Engineering Analysis of Reattaching Shear Layer Heat Transfer," AIAA Paper 72-717, June 1972.

[11]Ames Research Staff, "Equations, Tables, and Charts for Compressible Flow," NACA Report 1135, 1953.

[12]Bertin, J. J. and Cline, D. D., "Variable Grid-Size Transformations for Solving Nonsimilar Laminar and Turbulent Boundary Layers," *Proceedings of the 27th Heat Transfer and Fluid Mechanics Institute,* June 1980.

[13]Cebeci, T. and Smith, A. M. O., *Analysis of Turbulent Boundary Layers,* Academic, New York, 1974.

[14]Matthews, R. K., Nutt, K. W., Wannenwetsch, G. D., Kidd, C. T., and Boudreau, A. H., "Developments in Aerothermal Test Techniques at the AEDC Supersonic/Hypersonic Wind Tunnels," AIAA Paper 85-1003, June 1985.

[15]Eckert, E. R. G., "Engineering Relations for Friction and Heat Transfer to Surfaces in High Velocity Flow," *Journal of the Aeronautical Sciences,* Vol. 22, Aug. 1955, pp. 585–587.

[16]Hahn, M., "Experimental Investigation of Separated Flow Over a Cavity at Hypersonic Speed," *AIAA Journal,* Vol. 7, June 1969, pp. 1092–1098.